

**AN EXPERIMENTAL STUDY ON CORRELATIONS BETWEEN
CAVITATION EROSION RESISTANCE AND MECHANICAL
PROPERTIES FOR STAINLESS STEEL**

Peng Kewen, Li Gensheng, Tian Shouceng, Huang Zhongwei, Peng Chi, Nie Xiaokang
State Key Laboratory of Petroleum Resources and Prospecting, China U. of Petroleum
Beijing, Beijing 102249, China

ABSTRACT

It is well known that severe cavitation often leads to the breakdown of the performance of hydraulic equipment. Thus it is important to predict the cavitation erosion resistance when choosing materials. One feasible and convenient way is to correlate the cavitation erosion resistance with the mechanical properties, which can be measured by the simple indentation test. In this research, a series of cavitation erosion tests are conducted in a standard ASTM G134 cavitating jet apparatus. Stainless steel SUS630 is heat treated differently and used as specimens. Based on the experimental results, some useful correlations are presented. It is found out that yield stress, elastic work ratio, and hardness show similar power relationship with cavitation erosion resistance. The power exponent is 5.4, 4.4, and 3.5, respectively. The specimen being aged at 620°C shows resistance recovery during advanced erosion stage. The mechanism for this recovery is analyzed by X-ray diffraction.

1 INTRODUCTION

Cavitation refers to the formation of bubbles in the fluid when the local pressure drops below the saturated vapor pressure. The collapse of the cavitation bubbles is extremely violent and accompanied by high temperature and pressure in short duration. As a result, erosion on the material in the vicinity of cavitation collapse has been a severe concern for hydraulic equipment (Karimi and Martin). The mechanism of cavitation erosion is complicated and involves physical processes including bubble collapse and material responses to the impact (Kim et al.). Therefore, constant efforts have been devoted to this subject and one principal purpose is to develop high resistant materials.

To improve the material's cavitation erosion resistance (CER), heat treatment has been adopted for a long history. Various treatment methods have been used, such as annealing, aging, and sensitization. To evaluate CER under different heat treatment, erosion experiment is usually performed using a standard test apparatus such as ASTM G32 and ASTM G134. However, it may not be feasible or economical to perform a standard erosion test in certain circumstances since the test needs specific equipment and the considerable time. Instead, it is noticed that mechanical parameters are usually closely correlated with CER. For example, Hattori and Ishikura (Hattori and Ishikura) proposed that hardness is a reliable parameter to predict cavitation erosion resistance for stainless steel as CER increases with the 2.4th power of Vickers Hardness. Shin et al. (Shin et al.) considered the compressive strength and fracture strain are two important parameters enhancing the CER of Fe-based steel, even though the $\gamma \rightarrow \alpha'$ phase transformation decreased when the concentration of Cr was increased. Będkowski et al. (Będkowski et al.) pointed out that there is a linear relationship between CER and fatigue strength when plotting the curve in a dual logarithmic coordinate system figure. Another parameter showing a close relationship with CER is the reversible indentation work W_e done in an indentation test. dos Santos et al. (dos Santos, Garzón and Tschiptschin) displayed that incubation time increases with W_e , showing the material with higher W_e absorb less plastic energy under cavitation impact and thus has higher CER. However, for the variations of CER and mechanical properties caused by heat treatment, whether similar correlations exist is still an open issue and deserves to be studied.

In this paper, systemic investigations are conducted to study the cavitation erosion resistance under different heat treatment and examine its correlation with mechanical properties. The materials we choose is the widely used stainless steel SUS630, which is heat treated at different temperatures. Besides, the CER of SUS316L is also examined and compared to evaluate the treatment effect of SUS630. The erosion test is performed with an apparatus complying with the ASTM G134. The mechanical properties are obtained with an inverse analysis method based on indentation tests. Our results show that strong correlations exist between CER and three mechanical parameters, i.e. yield stress, hardness and elastic work ratio. Based on the conclusion from the erosion test, we also identify the optimum heat treatment scheme which enhances the CER of SUS630 most. The results from the present study provide references in evaluating the heat treatment effect for stainless steels.

2. EXPERIMENTAL DETAILS

2.1 Cavitating Jet Apparatus

The cavitating jet erosion system used in the present test complies with ASTM G134 (ASTM, G134-95) as displayed in Fig.1. Ion-exchange water is stored in tank A for at least 24 h before the experiment to keep the nuclei constant. Water temperature is kept at 297 ± 2 K during the test by the chiller connected to tank B. A plunger pump is used to inject the water into the nozzle to generate the submerged cavitating jet in the test section. Inside the test section, the metallic specimen is placed perpendicularly to the cavitating jet at a certain standoff distance s measured from the upstream corner of nozzle throat. Between the nozzle and specimen, there is a shutter separating the specimen from the jet while the test conditions are being set up. The water then flows out of the test section and recirculates back to tank A. The nozzle's upstream pressure p_1 is controlled by the rotation speed of the pump's inverter motor and downstream pressure p_2 is adjusted by the opening of the downstream valve.

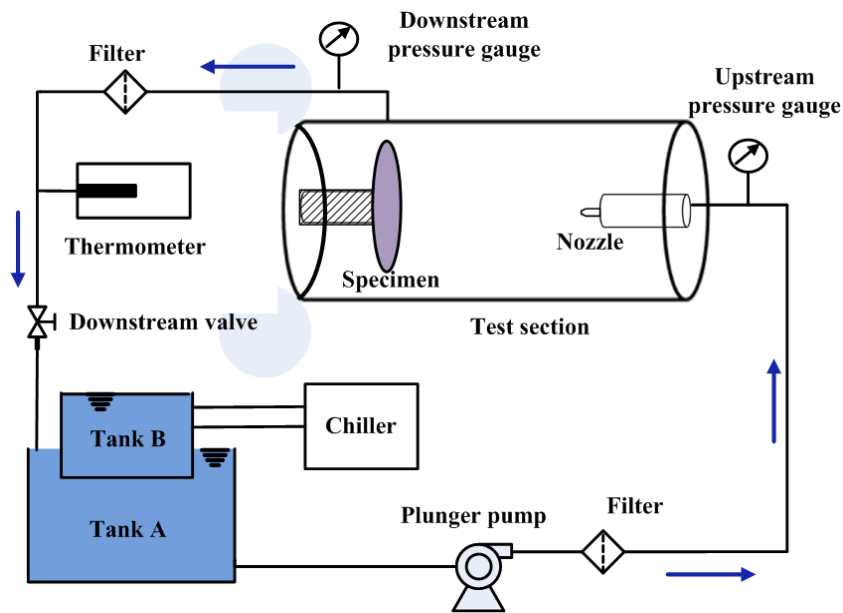


Figure 1. Schematic Diagram of the Cavitating Jet Apparatus

The standard nozzle for the ASTM G134 is used in the erosion test. The nozzle is cylindrical with the bore diameter $=0.4$ mm and the discharge coefficient $C_d=0.65$. The specimen is in the shape of a button. The surface subjected to cavitating jet impact is 12 mm in diameter and carefully polished to ensure the roughness $R_a<0.1\mu\text{m}$.

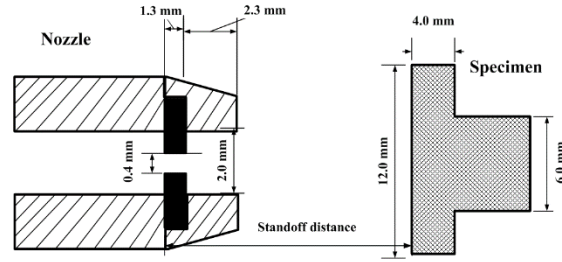


Figure 2. Schematic Diagrams of the Nozzle and Specimen

Table 1. Chemical composition of the specimens (wt.%)

Element	C	Si	P	S	Cu	Ni	Cr	Nb	Mn	Co	Mo	Fe
SUS630	0.04	0.3	0.23	0.09	3.2	4.63	15.4	0.3	-	0.1	-	balance
SUS316	0.01	0.1	0.03	0.01	-	12.0	16.7	-	1.6	-	2.0	balance
L	2	9	4	5	-	2	4	-	2	-	1	d

Based on the previous work (Soyama), the maximum cavitation erosion intensity of the jet is achieved at cavitation number $\sigma=0.014$ and standoff distance $s=19$ mm. In the present experiment, such a cavitation number was achieved with $p_1=30$ MPa and $p_2=0.42$ MPa.

2. 2 Materials and Mechanical Properties

Table 1 shows the chemical composition of the SUS630 and SUS316L specimens used in the present tests. The specimens are cylindrical with the smooth bottom surface to be subjected to the cavitating jet impact. For the specimen SUS630, each specimen is heat treated differently as illustrated in Table 3. Specimen A is solution annealed at 1040°C for 30 min followed by air cooling to the room temperature and is denoted as Condition A. Specimens B to E are annealed first under the same condition, then they are aged for 3 hours at different temperatures of 480°C , 550°C , 580°C and 620°C , respectively. According to the aging temperatures employed, these specimens are denoted as H900, H1025, H1075 and H1150, respectively.

Table 2. Heat treatment schemes of SUS630 specimens

Specimen	Heat treatment procedure		
	Solution annealing	Aging hardening	Type of cooling
A	1040 $^{\circ}\text{C}$, 30 min	Unaged (Condition A)	Air cooling
B		480 $^{\circ}\text{C}$ (H900), 3 h	
C		550 $^{\circ}\text{C}$ (H1025), 3 h	

D		580°C(H1075), 3 h	
E		620°C(H1150), 3 h	

Cavitation impact resulted from microjet or/and the pressure wave is highly localized, which prompts us to extract the specimen's mechanical properties from a micro-indentation test, rather than the conventional tensile test. The surface of the specimen for indentation is ground with emery paper up to 2000 grit and further polished by diamond paste of 0.1 μm particle size. The indentation tests are conducted using an ENT1100a indentation tester (Elionix Corp.) with the Vickers indenter. The maximum load is 200 mN and the loading rate is 20 mN/s. For each surface, 7 indentations at different spots are conducted. After obtaining the load-displacement P - h curve, the mechanical properties are extracted with the inverse method (Nishikawa and Soyama; Takakuwa, Mano and Soyama), where a response surface is constructed for the inverse calculation. The results are listed in Table 3.

Table 3. Mechanical parameters of the tested specimens

Materials	Specimen	Hardness H_v [GPa]	Yield stress σ_Y [GPa]	Elastic work ratio δ_e
	Condition A	3.31±0.03	0.97±0.02	0.415±0.01
	H900	4.67±0.04	1.17±0.02	0.531±0.02
SUS630	H1025	4.27±0.03	1.07±0.02	0.487±0.02
	H1075	3.92±0.05	1.03±0.01	0.457±0.01
	H1150	3.22±0.03	0.83±0.01	0.408±0.01
SUS316L	---	1.52±0.06	0.29±0.03	0.275±0.03

Table 3 also includes a parameter named plastic work ratio, which is also obtained from indentation test. The total deformation under indentation consists of the reversible part and irreversible part. The former recovers after the load is removed and the latter is responsible for the pits formed on the surface. Thus the elastic work ratio, δ_e , defined as the reversible work, W_e , to the total work, W_t , during indentation, represents the material capability to absorb energy without arousing permanent deformation. The elastic work ratio was calculated based on Fig.3, where W_e and W_t are represented by the area of the unloading section and the loading section, respectively.

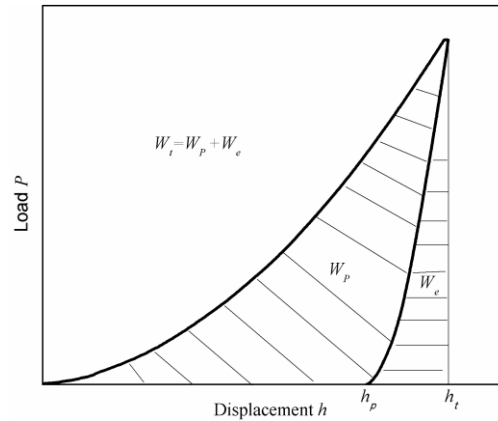


Figure 3. Schematic diagram showing elastic W_e and plastic work W_p done during the indentation test

2.3 X-ray diffraction

To examine the influence of microstructure on the material's erosion resistance, X-ray diffraction analysis is performed on a D8 ADVANCE Diffractometer (Bruker Corporation) using Cu-K α radiation. The scanned range of 2θ is 40° - 50° with the scan step of 0.017° , which is used to detect the austenite and martensite phase followed the suggestions from (Bhambroo et al.).

3. RESULTS AND DISCUSSION

In this section, the material's cavitation erosion intensity is analyzed based on the mass loss data from the tests. During the experiment, the mass loss was measured with the time interval of 10 min. Fig.4 and Fig.5 show the cumulative mass loss and mass loss rate as a function of exposure time, respectively. The data scatter from the test is within 5% and good repeatability is achieved. The curves in Fig 5 corresponds well with the typical cavitation erosion curve (ASTM, G134-95), which displays four erosion stages: incubation period, acceleration period, maximum rate period and deceleration period. Because of the large time interval adopted in weight measurement, the incubation stage, defined as the exposure time prior to the noticeable mass loss, cannot be discerned from those curves. However, these curves can still clearly display the significant disparities in erosion resistance among the different specimens.

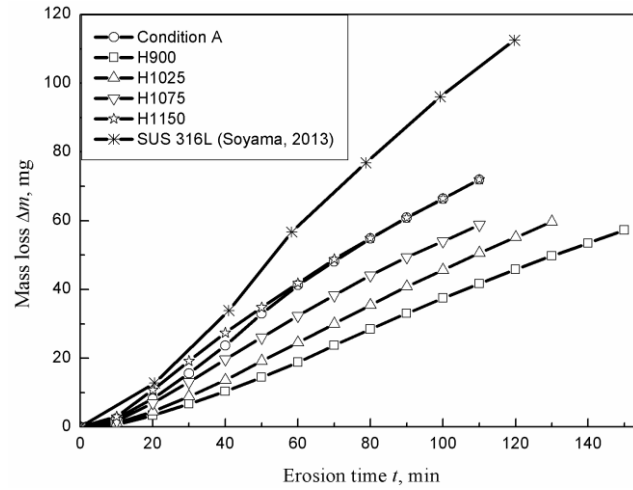


Figure 4. Cavitation erosion mass loss different specimens

Following the recommendation of the ASTM G134 standard, the reciprocal of the maximum cumulative erosion rate, E_{Rmax} , is defined as the cavitation erosion resistance of the material. The material shows decreasing cavitation erosion resistance in the order of H900, H1025, H1075, Condition A, H1150 and SUS316L. In addition, the time needed to attain the peak erosion rate increases with increasing erosion resistance. For example, it takes 130 minutes for the most resistant specimen H900 to attain the maximum erosion rate of 0.38 mg/min, while only 60 minutes is needed for the least resistant specimen SUS316L to reach the peak rate of 0.97 mg/min. Besides, the duration of each erosion stage also shows resistance-dependent features. Specifically, the maximum rate period is much longer for high resistant specimens such as H900 and H1025, while for the low resistant specimens H1150 and SUS316L, the erosion proceeds into the deceleration period immediately following the peak erosion rate.

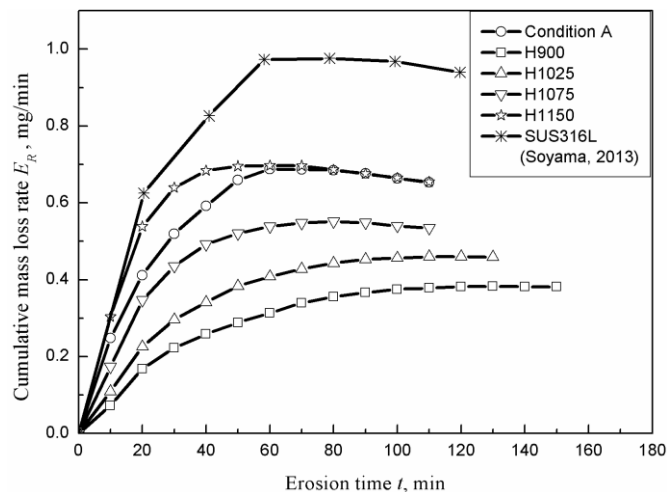


Figure 5. Cavitation erosion mass loss rate for different specimens

The specimen H1150 shows interesting time varying erosion feature as illustrated in Fig.10, where the mass loss ratio between H1150 and H900, as well as the mass loss ratio between H1150 and Condition A, is plotted against the erosion time. Both the two curves in Fig.6 decline

with erosion time and approach an asymptotic value, which is 1.7 and 1.0, respectively. This feature indicates that the instant cavitation erosion resistance of H1150 recovers in advanced erosion stage. The mechanism for this phenomenon will be discussed later.

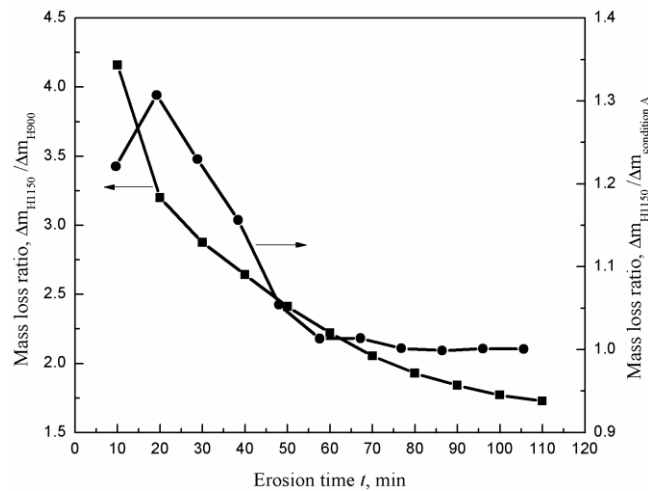


Figure 6. Time-varying erosion mass loss ratio of specimen H1150 in relation to specimen H900 and specimen Condition A

Yield stress σ_Y is defined the stress at which the material begins to deform plastically and is an important parameter to evaluate the material's strength. For the brittle and high-strength stainless steel such as SUS630 and SUS316, permanent deformation and subsequent material failure would occur if the applied stress is beyond σ_Y . Cavitation collapse often produces impacts in the order of GPa, which is far larger than σ_Y . Therefore, it is expected that the material's cavitation erosion resistance R_E is closely related to yield stress σ_Y . Fig.7 proves this assumption and shows that R_E increases with σ_Y to the power of 5.4. The coefficient of determination $R^2=0.928$ by performing the least square fitting. Thus the indentation-induced yield stress is a good indicator for predicting the CER of stainless steel. Besides, since both cavitation impact and indentation load are compressive and highly concentrated on the material's surface, the inverse analysis method which calculates yield stress inversely from indentation curve shows its superiority, as demonstrated by the high fitting coefficient.

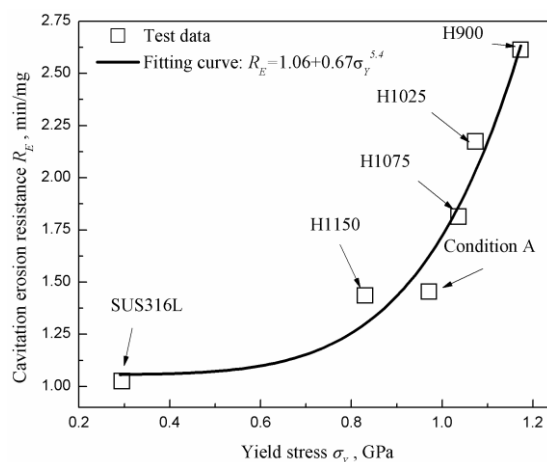


Figure 7. Correlation between cavitation erosion resistance and yield stress

Compared with the yield stress σ_Y , the elastic work ratio δ_e reflects more specifically how much energy the material can absorb before deforming plastically under external loads. Thus it is another reliable parameter representing the cavitation erosion resistance R_E , as illustrated in Fig.8. It shows that R_E increases with δ_e to the power of 4.4, which is close to the power exponent 5.4 for the correlation between R_E and σ_Y .

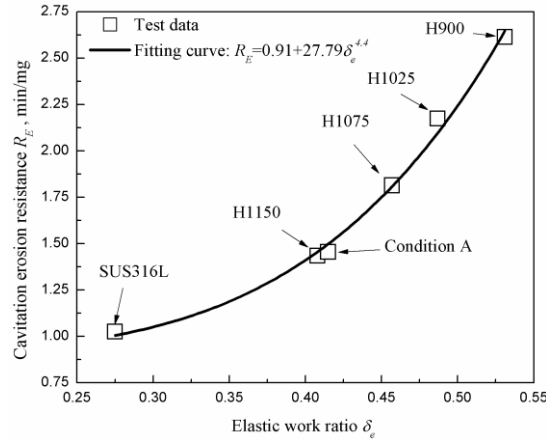


Figure 8. Correlation between cavitation erosion resistance and elastic work ratio

Unlike yield stress, hardness evaluates the material's resistance to plastic deformation. Fig.9 shows the correlation between the value of Vickers hardness H_v and cavitation erosion resistance R_E , where R_E increases with H_v to the power of 3.5. Compared with yield strength, the fitting between R_E and H_v gives the higher coefficient of determination, i.e. $R^2=0.997$, which is surprisingly satisfactory. While yield stress measures the material's upper limit of elastic deformation, hardness evaluates how resistant the material is to permanent deformation, which relates to material failure under cavitation impact more closely. Therefore, the correlation coefficient regarding H_v is higher than that regarding σ_Y .

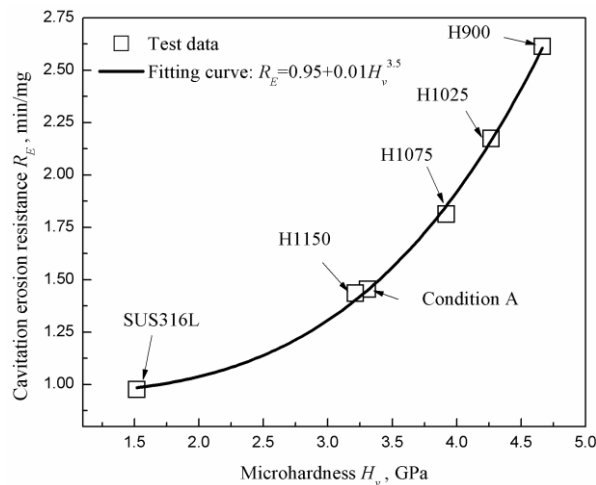


Figure 9. Correlation between cavitation erosion resistance and microhardness

With respect to the recovery of erosion resistance for specimen H1150 during the erosion process, X-ray diffraction analysis is performed before and after erosion test to examine the

microstructural evolution. Since the eroded surface becomes rather roughed after prolonged erosion, the comparative test is conducted on the surface after exposure to cavitating jet impact for 30 min. The black curve in fig.10 corresponds to result before erosion test and the red curve corresponds to that after being impacted for 30 min. It is seen that the black curve confirms the existence of the austenite phase in a small fraction, which is reverted under high aging temperature. After being impacted by cavitating jet for 30 minutes, the content of the austenite phase is reduced to be negligible as demonstrated by the red curve. Thus it is concluded that there exists phase transformation from austenite to martensite for the H1150 specimen under cavitation impact. It was previously demonstrated by (Wang and Zhu) and (Park et al.) that the transformation itself absorbs a fraction of the impact energy, thus reducing the erosion of the materials. Besides, the newly formed martensitic phase has higher erosion resistance to cavitation impact compared with the original austenitic phase according (Heathcock, Protheroe and Ball) and (Karimi and Martin). With the above reasoning, it is expected that the phase transformation is responsible for the recovery of erosion resistance for the H1150 specimen.

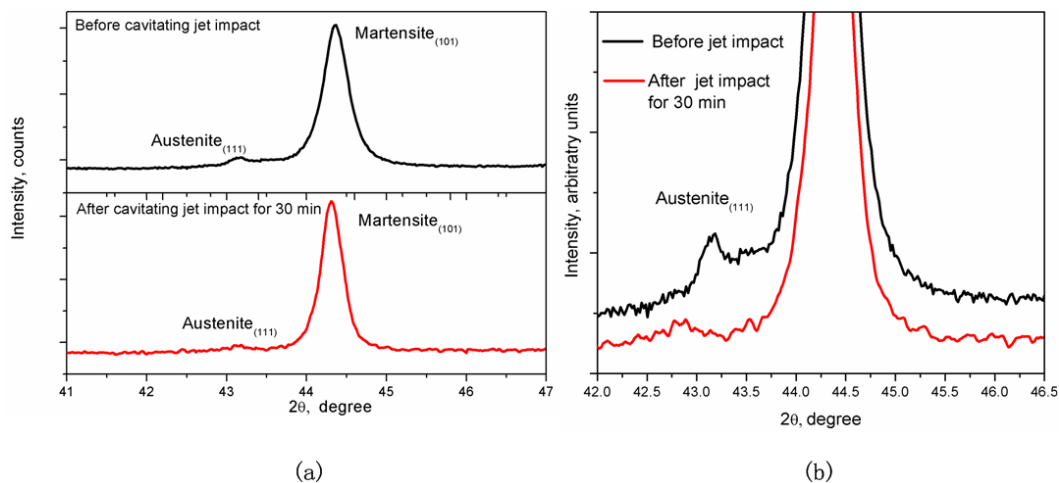


Figure 10. (a) X-ray diffraction patterns for specimen H1150 and (b) close-up showing the variation of austenite phase content

4. CONCLUSION

In order to examine the correlation between cavitation erosion resistance and mechanical properties for stainless steel SUS630 under different heat treatment, cavitation erosion tests are conducted with a cavitating jet apparatus, which is compliant with the ASTM G134 standard. An inverse analysis method based on indentation tests are employed to calculate the materials' mechanical properties. The main conclusions are summarized as follows:

1. The parameters of yield stress σ_Y , elastic work ratio δ_e and hardness H_v are proved to be good indicators for predicting the material's cavitation erosion resistance under heat treatment. All the three parameters show power relationship with cavitation erosion resistance R_E . The power exponent is 5.4, 4.4 and 3.5, respectively.
2. The material SUS630 H1150 shows recovery of cavitation erosion resistance during the erosion process. The phase transformation from austenite to martensite is assumed to be responsible for the recovery.

ACKNOWLEDGEMENTS

This work is supported by Newton Fund-China-UK Research and Innovation Bridges (NO.S2016G7261), National Natural Science Foundation of China (NO.U1562212) and China Scholarship Council (NO.201606440089).

REFERENCES

- ASTM, G134-95. Standard Test Method for Erosion of Solid Materials by a Cavitating Liquid Jet. Annual Book of ASTM Standards.
- Będkowski, W, et al. "Relations between Cavitation Erosion Resistance of Materials and Their Fatigue Strength under Random Loading." *Wear* 230.2 (1999): 201-09. Print.
- Bhambroo, Rajan, et al. "Effect of Reverted Austenite on Mechanical Properties of Precipitation Hardenable 17-4 Stainlesssteel." *Materials Science and Engineering: A* 568 (2013): 127-33. Print.
- dos Santos, José Francisco, Carlos Mario Garzón, and André Paulo Tschiptschin. "Improvement of the Cavitation Erosion Resistance of an Aisi 304l Austenitic Stainless Steel by High Temperature Gas Nitriding." *Materials Science and Engineering: A* 382.1 (2004): 378-86. Print.
- Hattori, Shuji, and Ryohei Ishikura. "Revision of Cavitation Erosion Database and Analysis of Stainless Steel Data." *Wear* 268.1 (2010): 109-16. Print.
- Heathcock, CJ, BE Protheroe, and A Ball. "Cavitation Erosion of Stainless Steels." *Wear* 81.2 (1982): 311-27. Print.
- Karimi, A, and JL Martin. "Cavitation Erosion of Materials." *International Metals Reviews* 31.1 (1986): 1-26. Print.
- Kim, Ki-Han, et al. *Advanced Experimental and Numerical Techniques for Cavitation Erosion Prediction*. Vol. 106: Springer, 2014. Print.
- Nishikawa, Masaaki, and Hitoshi Soyama. "Two-Step Method to Evaluate Equibiaxial Residual Stress of Metal Surface Based on Micro-Indentation Tests." *Materials & Design* 32.6 (2011): 3240-47. Print.
- Park, Myung Chul, et al. "Effects of Strain Induced Martensitic Transformation on the Cavitation Erosion Resistance and Incubation Time of Fe–Cr–Ni–C Alloys." *Wear* 274 (2012): 28-33. Print.
- Shin, Gyeong Su, et al. "Effect of Mechanical Properties on Cavitation Erosion Resistance in $\alpha \rightarrow \beta'$ Phase Transformable Fe – Cr–C–Mn Alloys." *Tribology Letters* 57.3 (2015): 25. Print.
- Soyama, Hitoshi. "Effect of Nozzle Geometry on a Standard Cavitation Erosion Test Using a Cavitating Jet." *Wear* 297.1 (2013): 895-902. Print.
- Takakuwa, O, Y Mano, and H Soyama. "Increase in the Local Yield Stress near Surface of Austenitic Stainless Steel Due to Invasion by Hydrogen." *International Journal of Hydrogen Energy* 39.11 (2014): 6095-103. Print.
- Wang, Zaiyou, and Jinhua Zhu. "Effect of Phase Transformation on Cavitation Erosion Resistance of Some Ferrous Alloys." *Materials Science and Engineering: A* 358.1 (2003): 273-78. Print.